Geochemical Perspectives Letters

Neodymium isotopes trace marine provenance of Arctic sea ice

G. Laukert[1,2,3*], I. Peeken[4], D. Bauch[5], T. Krumpen[4], E.C. Hathorne[1], K. Werner[4,6], M. Gutjahr[1], M. Frank[1]

https://doi.org/10.7185/geochemlet.2220

Abstract

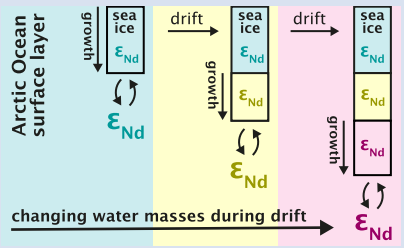

Radiogenic neodymium (Nd) isotopes (ε_{Nd}) have the potential to serve as a geochemical tracer of the marine origin of Arctic sea ice. This capability results from pronounced ε_{Nd} differences between the distinct marine and riverine sources, which feed the surface waters from which the ice forms. The first dissolved Nd isotope and rare earth element (REE) concentration data obtained from Arctic sea ice collected across the Fram Strait during RV *Polarstern* cruise PS85 in 2014 confirm the incorporation and preservation of the parental surface seawater ε_{Nd} signatures despite efficient REE rejection. The large ε_{Nd} variability between ice floes and within sea ice cores (−32 to −10) reflects changes in water mass distribution during ice growth and drift from the central Arctic Ocean to Fram Strait. In addition to the parental seawater composition, our new approach facilitates the reconstruction of the transfer of matter between the atmosphere, the sea ice and the ocean. In conjunction with satellite-derived drift trajectories, we enable a more accurate assessment of sea ice origin and spatiotemporal evolution, benefiting studies of sea ice biology, biodiversity, and biogeochemistry.

Received 6 January 2022 | Accepted 5 May 2022 | Published 10 June 2022

Introduction

The ongoing decrease in the age, thickness and extent of Arctic sea ice cover is projected to strongly impact climate, weather, ecosystems, matter fluxes and human activities in the near future (IPCC, 2022). The transition from a perennial ice cover with major sea ice transport systems to a seasonally ice-free ocean with isolated ice fields and floes of different origin is already impacting the distribution of gaseous, dissolved, and particulate matter, with far reaching consequences for Arctic ecosystems and biogeochemical cycles (*e.g.*, Krumpen *et al.*, 2019). Accurate knowledge of sea ice origin and drift is therefore required to understand the changing role of the marine cryosphere in regulating matter fluxes and ecological processes.

Satellite-based sea ice motion products are currently the only available resource for reconstructing sea ice origin and drift trajectories (Krumpen *et al.*, 2021). However, these mainly provide information about ice and atmospheric conditions, while the water mass distribution during ice growth and drift remains unexplored. Biological and biogeochemical processes in sea ice are, however, tightly linked to the parental seawater composition. Geochemical provenance tracers have the potential to reveal this composition as well as biogeochemical atmosphere-ice-ocean exchange during drift, thus ideally complementing satellite-based observations.

Radiogenic neodymium (Nd) isotopes (expressed as $\varepsilon_{Nd} = (^{143}Nd/^{144}Nd)_{sample}/(^{143}Nd/^{144}Nd)_{CHUR} - 1\} \times 10^4$, with CHUR = 0.512638; Jacobsen and Wasserburg, 1980) are a powerful tracer of water mass mixing and ocean circulation (Frank, 2002), but their application as a tracer of the water masses from which sea ice forms is novel. This potential results from the incorporation of small amounts of Nd from the ocean surface layer into sea ice during sea ice growth (Laukert *et al.*, 2017c). Due to salt-proportional rejection, the concentrations of Nd and other rare earth elements (REEs) in sea ice drop below those of seawater. This makes precise and accurate ε_{Nd} analysis difficult but can be compensated for by larger sample volume.

In the Arctic Ocean, the ε_{Nd} signature of surface waters reflects contributions from water masses and major rivers and ranges between −17 and −5.5 (see Fig. S-1 and description of marine ε_{Nd} systematics in the Supplementary Information; Andersson *et al.*, 2008; Porcelli *et al.*, 2009; Laukert *et al.*, 2017a, 2017b, 2017c, 2019; Paffrath *et al.*, 2021). Significantly less radiogenic ε_{Nd} signatures (<−17) are only introduced *via* discharge from Greenland and the Canadian Arctic Archipelago (Filippova *et al.*, 2017; Laukert *et al.*, 2018; Grenier *et al.*, 2022). Four ice floes sampled in the central Arctic Ocean in 2012 had ε_{Nd} compositions similar to their parental waters (Laukert *et al.*, 2017c), pointing to the incorporation of seawater ε_{Nd} signatures during sea ice growth. However, these samples

1. GEOMAR Helmholtz Centre for Ocean Research, Kiel, Germany
2. Department of Oceanography, Dalhousie University, Halifax, Canada
3. Woods Hole Oceanographic Institution, Woods Hole, USA
4. Alfred Wegener Institute, Helmholtz Centre for Polar and Marine Research, Bremerhaven, Germany
5. Christian-Albrecht University of Kiel, Kiel, Germany
6. University of Rostock, Rostock, Germany
* Corresponding author (email: georgi.laukert@dal.ca)

were unfiltered and direct contributions from particulate phases could not be excluded.

To further explore the suitability of Nd isotopes for tracing the marine origin of sea ice, we determined dissolved Nd isotopes along with salinity, temperature, stable oxygen isotopes and the complete set of REEs in different sea ice cores collected from ice floes in Fram Strait during cruise PS85 of RV *Polarstern* in 2014. Comparison with snow cover and surface seawater properties as well as ice drift trajectories reconstructed with IceTrack (Krumpen *et al.*, 2019) allows us to significantly expand our knowledge of the mechanisms controlling ε_{Nd} in the marine cryosphere.

Tracer Data and Satellite-Based Sea Ice Origin

The tracer data were determined in sea ice and snow samples collected from nine sea ice floes of different sizes, ages, and origins across Fram Strait as well as in nearby surface seawater (Fig. 1; see Supplementary Information for methodology and data). Based on visual inspection, the ice cores and the filters used for filtration of the melted sea ice samples were free of ice rafted detrital material. The dissolved ε_{Nd} of the sea ice ranges between −31.6 and −10.1, while less variability is observed in snow and surface seawater (average $\varepsilon_{Nd} = -14.7 \pm 1.0$ and -11.1 ± 0.7, respectively; 1 s.d., $n = 7$). The least radiogenic ε_{Nd} compositions were determined in the lowermost ice core intervals at stations 419, 454 and 472 and correspond to highest Nd concentrations ([Nd]) and the lowest heavy (H) to light (L) REE ratios normalised to PAAS (Post Archaean Australian Shale $\times 10^6$; see Supplementary Information) (Fig. 1). A low HREE/LREE ratio generally indicates exchange with freshly weathered rock material and is characteristic of freshwater that has been recently discharged to the ocean (*e.g.*, Laukert *et al.*, 2017a). [Nd] and HREE/LREE in our sea ice correlate well with ε_{Nd} ($R^2 = 0.75$ and 0.86, respectively; Fig. 2a,b). A correlation is also observed between HREE/LREE and ε_{Nd} ($R^2 = 0.7$) for surface seawater despite the smaller range in ε_{Nd} compositions. In contrast, no significant correlations between any of these parameters exist for the snow samples. On average, REE patterns from sea ice are similar in the dissolved (<0.45 µm) and truly dissolved (<3 and 30 kDa) size fractions, exhibiting LREE depletion and negative Ce anomalies, whereas REE patterns in snow are much flatter, consistent with the origin of REEs from atmospheric aerosols (Figs. S-2, S-3). The truly dissolved REE concentrations of sea ice average ~85 % of the dissolved REEs, except at station 481 where only ~55 % of the dissolved REEs were present in the truly dissolved pool. In snow, the truly dissolved concentrations average 50–60 % of the dissolved REEs. The dissolved [REE] in sea ice on average correspond to only 10–30 % of the dissolved [REE] of Arctic surface seawater.

The stable oxygen isotope signatures ($\delta^{18}O$) of the sea ice range from −5.8 to −0.7 ‰ at an average salinity of 3.6 ± 0.8 (1 s.d., $n = 29$). Melting of sea ice is evidenced by near zero salinities only for the upper 50 cm of station 481 and the uppermost 10 cm of stations 461 and 472 (Fig. S-4). The snow samples have more negative $\delta^{18}O$ values reaching ~−23 ‰ and salinities approaching zero, consistent with atmospheric deposition. Neither salinity nor $\delta^{18}O$ in sea ice or snow correlate with [Nd], HREE/LREE or ε_{Nd} (Fig. 2c,d). Surface seawater $\delta^{18}O$ values are not available for our samples but likely range between −2.8 and +0.3 ‰ (Laukert *et al.*, 2017a).

Tracking of sea ice drift based on satellite data (see Supplementary Information) reveals that the ice floes of stations 419 and 426 originated from the nearby Norske Øer Ice Barrier (NØIB), a fast ice field that forms along East Greenland's coast and was sampled directly at station 408 (Fig. 1). The common origin of this ice is confirmed by similar temperature and salinity profiles, except at station 408 where near-freezing temperatures reflect direct sampling from the NØIB (Fig. S-4). According to IceTrack, all other ice floes originated from ice fields of the central Arctic Ocean transported *via* the Transpolar Drift (Fig. S-5). Exactly where and when the individual ice floes were formed along the drift route cannot be determined from IceTrack alone. However, the different ice thicknesses of these floes indicate that they must have formed at different times and places along the route.

Reconstructing Marine Provenance of Sea Ice and Atmosphere-Ice-Ocean Exchange

Our data show that the dissolved ε_{Nd} signature of surface seawater is incorporated into sea ice during growth and preserved during transport despite rejection of up to ~90 % of the seawater REEs. Most upper ice core intervals have an ε_{Nd} signature between −15 and −10 and a salinity normalised [Nd] of ~1 pmol, which is within the compositional range of surface seawater in the central Arctic Ocean (Fig. 3a) and hence in agreement with ice growth along the drift route reconstructed for the pack ice floes (Fig. S-5). We use the ratio of [Nd] and salinity ([Nd]/S) to correct for salt-proportional rejection of Nd, which enables direct comparison between sea ice and seawater (Laukert *et al.*, 2017c). The least radiogenic ε_{Nd} signatures reported to date for waters circulating in the vicinity of Greenland (~−24; Laukert *et al.*, 2018) are more positive than the values determined in the lower ice core intervals at stations 419, 454, and 472 (reaching ~−32). However, despite the lack of published seawater data with similarly low signatures, these likely were introduced from Greenland through erosion and weathering of metamorphic rocks with even lower ε_{Nd} reaching values of ~−42 (Laukert *et al.*, 2017a and references therein). Dissolved ε_{Nd} signatures of Canadian rivers draining the same lithologies in a similar glacial environment are as low as those in our ice cores and, due to the very high [Nd] and despite estuarine REE removal, likely extend well beyond coastal areas once introduced into the surface ocean (Grenier *et al.*, 2022). Similarly unradiogenic ε_{Nd} signatures are therefore expected for surface waters near Greenland that were incorporated into sea ice at the end of the Transpolar Drift at stations 419, 454, and 472. Alternatively, the partial dissolution of small labile particulate phases originating from Greenland and incorporated during sea ice formation and drift or during sample processing may explain the very negative signatures. However, the ice core intervals with these signatures have [Nd]/S and HREE/LREE/S values for a given ε_{Nd} similar to Greenland coastal waters or sea ice expected to form from them (Fig. 3; the slight offset between actual and expected HREE/LREE/S values in sea ice reflects a process discussed below), which strongly suggests that these signals reflect direct incorporation of Greenland meltwater. Besides, a contribution of Greenland-sourced particles to the sea ice signal would not change our interpretation, given that their distribution in surface waters will not be significantly different from that of Greenland-sourced meltwater.

At station 419, despite the proximity to the Greenland coast, surface seawater ε_{Nd} signatures were around −11 and thus differed markedly from the sea ice ε_{Nd} of −27.6. The ice floes from stations 454 and 472 originated from the central Arctic Ocean and have similar ice core lengths and ε_{Nd} distributions.

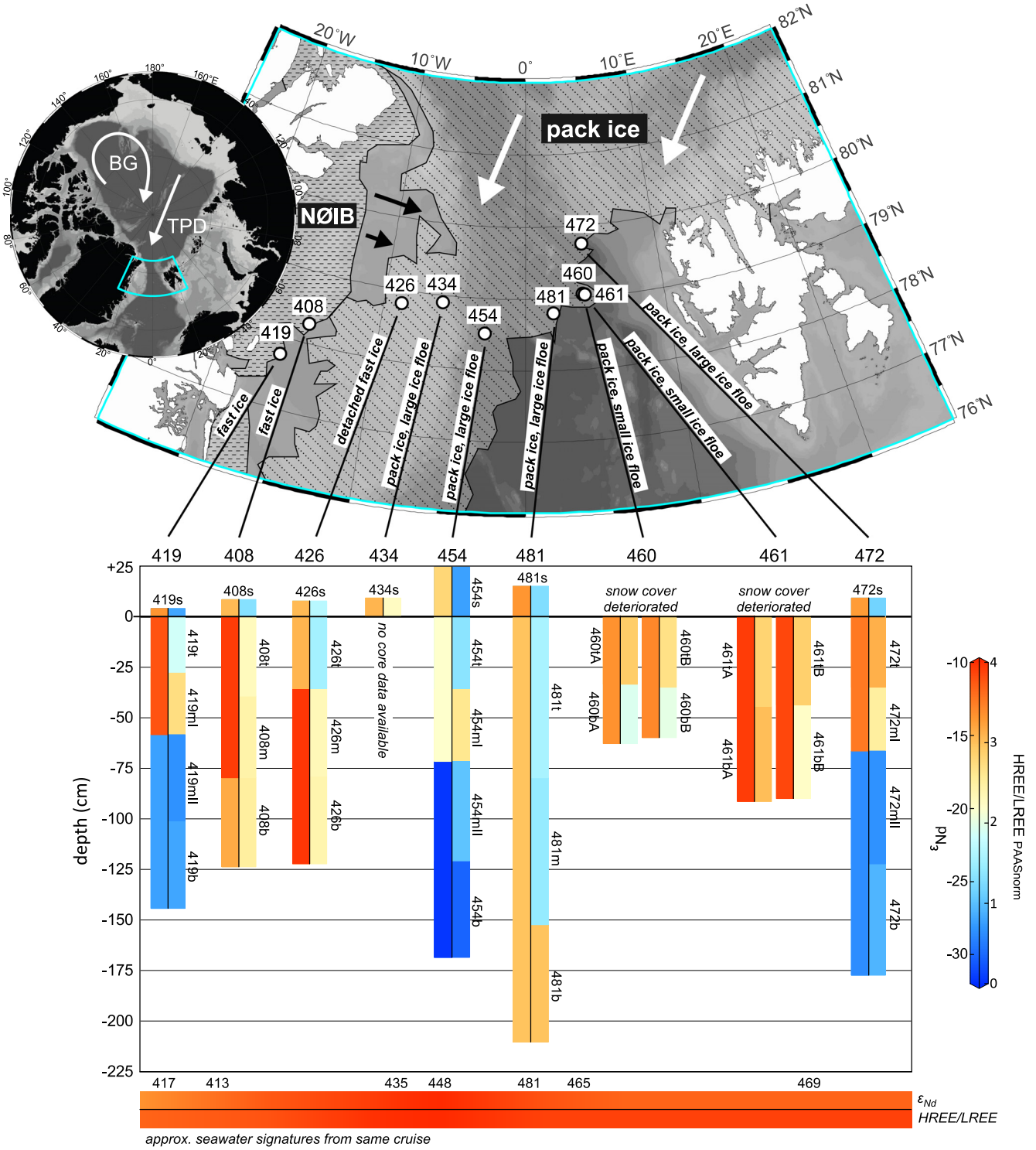

Figure 1 Locations of sea ice stations with approximate distribution of pack ice transported *via* the Transpolar Drift (TPD) and fast ice comprising the Norske Øer Ice Barrier (NØIB) in the Fram Strait in June 2014 obtained from satellite data. In addition, ice transport *via* the Beaufort Gyre (BG) is indicated in the overview map. Below, the ε_{Nd} (left bars) and HREE/LREE (right bars) distributions in snow cover and sea ice cores are shown together with surface seawater signatures of nearby stations (horizontal bar at the bottom).

They likely acquired their unradiogenic signatures from coastal waters advected to the area northeast of Greenland *via* the North-East Greenland Coastal Current (Laukert *et al.*, 2017a). The multi-year ice at station 419 thus likely originated from the same area before it attached to the NØIB prior to sampling. In contrast to ε_{Nd}, $\delta^{18}O$ is insensitive to Greenland meltwater incorporation due to indistinguishable $\delta^{18}O$ values in surface waters along the East Greenland coast and Arctic open ocean waters (> ~−3 ‰; Laukert *et al.*, 2017a).

The lower ice core interval at station 481 has some of the highest HREE/LREE of all cores, which argues against incorporation of Greenland meltwater. The ε_{Nd} signature of −15.5 thus can neither be entirely explained by meltwater incorporation nor by infiltration of snow meltwater (ε_{Nd} = −13.7). Instead, it most

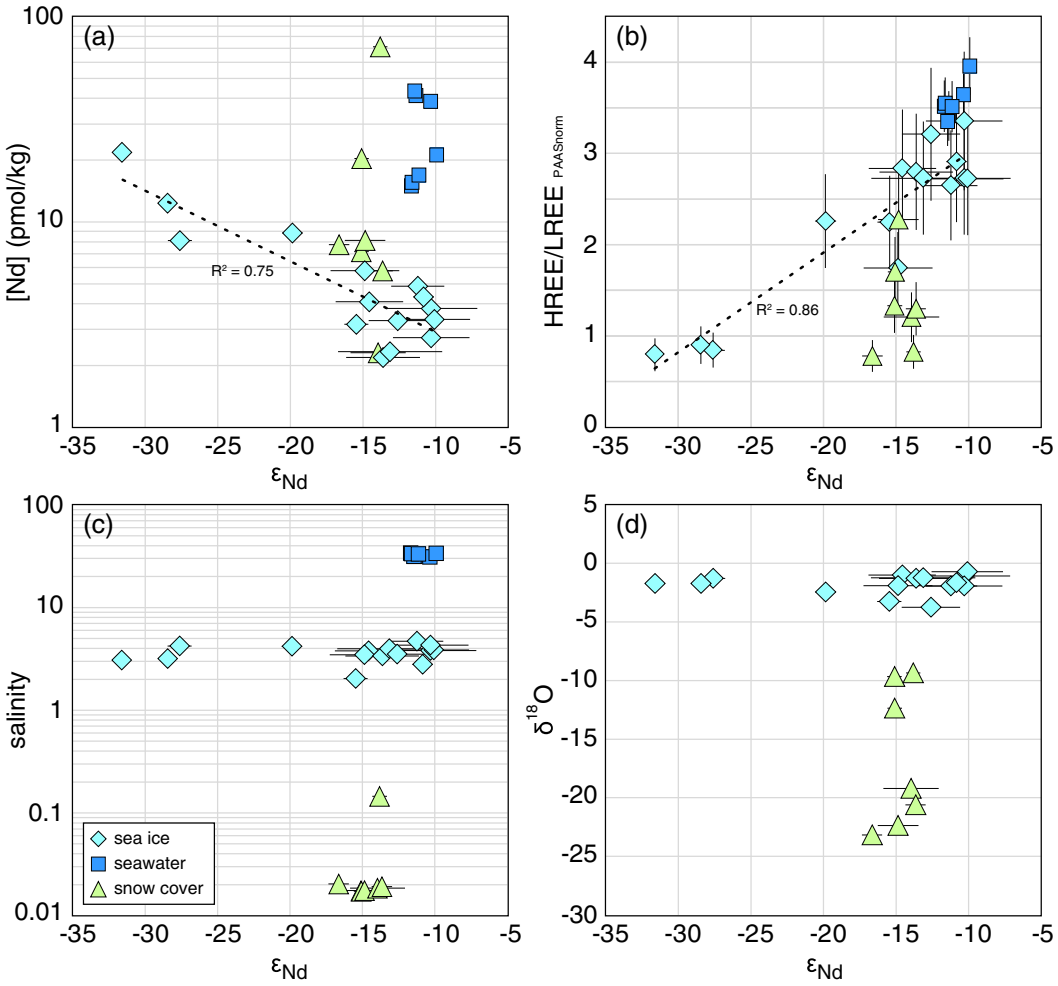

Figure 2 Comparison of ε_{Nd} with **(a)** [Nd], **(b)** HREE/LREE, **(c)** salinity and **(d)** $\delta^{18}O$ for all samples from this study.

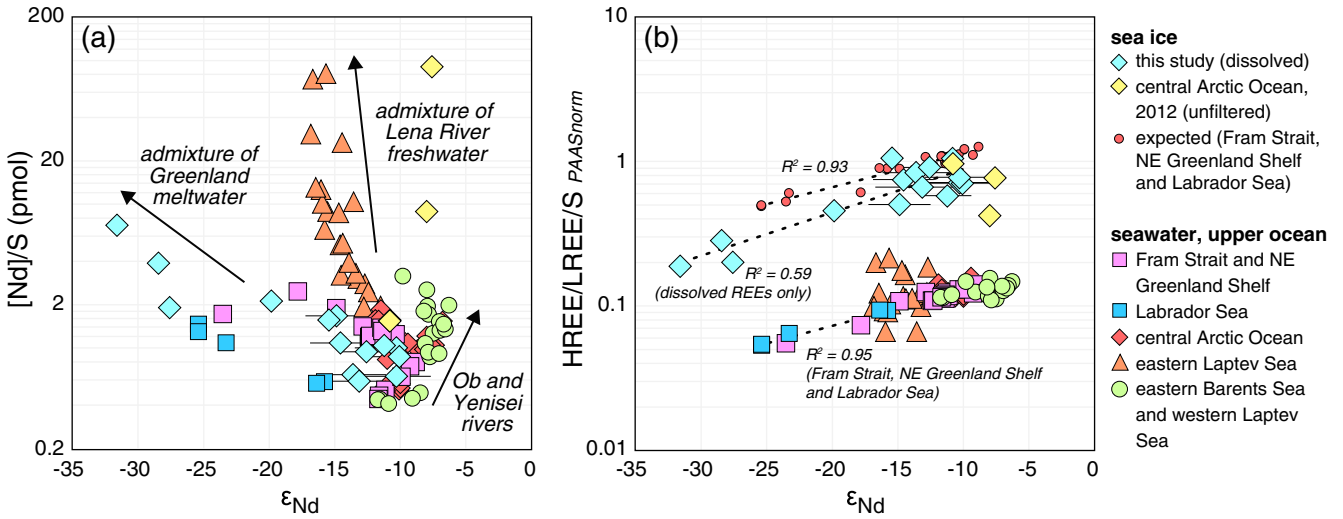

Figure 3 Comparison between ε_{Nd} and **(a)** [Nd]/S and **(b)** HREE/LREE/S for sea ice and seawater samples from this study and from the literature (see main text for references). Expected HREE/LREE/S values for sea ice were calculated by normalising seawater HREE/LREE values with the average salinity of the sea ice samples (3.6) instead of the seawater salinity.

likely reflects the uptake of Nd from Lena River freshwater characterised by an ε_{Nd} of ~−17 to ~−16 (Laukert *et al.*, 2017b). This is supported by a relatively low $\delta^{18}O$ value of −5.8 ‰ in the upper ice core interval and differences in the REE distribution between the different size fraction pools. The incorporation of a higher fraction of colloidal REEs (>30 kDa) at station 481 (~45 %) than at all other stations (~15 %) is consistent with incorporation of river-borne REEs and colloids from the Lena

River (Laukert *et al.*, 2017b). The near zero salinity in the upper ice core interval at this station indicates advanced melting from the previous year, also supporting the formation of this multi-year ice in the Laptev Sea and its long distance transport across the central Arctic Ocean.

The salt-normalised HREE/LREE values in sea ice are slightly lower than expected for a salt-proportional REE rejection with no change in the HREE/LREE ratio (Fig. 3b). The rejection is thus stronger for the HREEs than for the LREEs, which also explains the overall lower HREE/LREE ratios in sea ice compared to surface seawater. Despite the preferential rejection of HREEs, the differences in HREE/LREE between the parental source waters are maintained, as evidenced by a trend towards lower HREE/LREE/S values with decreasing ε_{Nd} in both sea ice and seawater. Lower HREE/LREE ratios were also observed in unfiltered sea ice samples from the central Arctic Ocean and were attributed to the contribution of particulate LREEs or differences in the incorporation of distinct size fraction pools (Laukert *et al.*, 2017c). Our dissolved and truly dissolved REE data allow us to exclude any direct contributions from particulate phases and instead indicate the elemental fractionation of dissolved REEs resulting from differential seawater/brine speciation. Preferential HREE rejection into the water column could also account for the accumulation of dissolved HREEs in bottom waters of the Laptev Sea (Laukert *et al.*, 2017b) but this requires further investigation in future dedicated process studies.

Conclusions

Our data demonstrate that Nd isotopes are a powerful tracer of the marine provenance of Arctic sea ice and biogeochemical atmosphere-ice-ocean exchange in combination with other source sensitive parameters. Even if exchange between sea ice and seawater immediately before sampling cannot be fully excluded at some stations due to indistinguishable ε_{Nd} signatures, the highly unradiogenic signatures of the Greenland-influenced ice floes suggest that, despite near zero temperatures, ε_{Nd} signatures of sea ice are largely preserved during periods in which the ice does not grow and even during periods of melting. Combined with satellite-derived sea ice motion products, our new approach enables a more accurate assessment of the water mass composition during sea ice growth and drift, which is essential for studies of sea ice formation and marine biology, biodiversity and biogeochemistry.

Author Contributions

GL and IP conceived the study. IP took the sea ice samples. TK reconstructed sea ice trajectories. GL prepared the samples and analysed Nd isotopes together with MG and rare earth elements together with EH. DB overlooked stable oxygen isotope sampling and analysis. All authors were involved in writing the manuscript, data interpretation and discussion.

Acknowledgements

We thank the Captain and Crew of the RV *Polarstern* for their help in collecting and transporting the samples and the chief scientist Ingo Schewe for his support (AWI_PS85_04). We also thank Antje Wildau for collecting the seawater samples and Ulrike Dietrich, Lars Chresten Lund-Hansen, Brian Keith Sorrell and Bibi Ziersen for their help with the sea ice work. Jutta Heinze is acknowledged for laboratory assistance. We acknowledge financial support by the German Federal Ministry of Education and Research (Grant BMBF 03F0776 and 03G0833) and the Ministry of Education and Science of the Russian Federation. GL also acknowledges financial support from the Ocean Frontier Institute through an award from the Canada First Research Excellence Fund. The authors declare no conflicts of interest relevant to this study.

Editor: Gavin Foster

Additional Information

Supplementary Information accompanies this letter at https://www.geochemicalperspectivesletters.org/article2220.

Cite this letter as: Laukert, G., Peeken, I., Bauch, D., Krumpen, T., Hathorne, E.C., Werner, K., Gutjahr, M., Frank, M. (2022) Neodymium isotopes trace marine provenance of Arctic sea ice. *Geochem. Persp. Let.* 22, 10–15. https://doi.org/10.7185/geochemlet.2220

References

Andersson, P.S., Porcelli, D., Frank, M., Bjork, G., Dahlqvist, R., Gustafsson, O. (2008) Neodymium isotopes in seawater from the Barents Sea and Fram Strait Arctic-Atlantic gateways. *Geochimica et Cosmochimica Acta* 72, 2854–2867. https://doi.org/10.1016/j.gca.2008.04.008

Filippova, A., Frank, M., Kienast, M., Rickli, J., Hathorne, E.C., Yashayaev, I.M., Pahnke, K. (2017) Water mass circulation and weathering inputs in the Labrador Sea based on coupled Hf–Nd isotope compositions and rare earth element distributions. *Geochimica et Cosmochimica Acta* 199, 164–184. https://doi.org/10.1016/j.gca.2016.11.024

Frank, M. (2002) Radiogenic isotopes: tracers of past ocean circulation and erosional input. *Reviews of Geophysics* 40, 1–38. https://doi.org/10.1029/2000RG000094

Grenier, M., Brown, K.A., Colombo, M., Belhadj, M., Baconnais, I., Pham, V., Soon, M., Myers, P.G., Jeandel, C., François, R. (2022) Controlling factors and impacts of river-borne neodymium isotope signatures and rare earth element concentrations supplied to the Canadian Arctic Archipelago. *Earth and Planetary Science Letters* 578, 117341. https://doi.org/10.1016/j.epsl.2021.117341

IPCC (2022) *Climate Change 2022: Impacts, Adaptation, and Vulnerability*. Contribution of Working Group II to the Sixth Assessment Report of the Intergovernmental Panel on Climate Change [Pörtner, H.-O., Roberts, D.C., Tignor, M., Poloczanska, E.S., Mintenbeck, K., Alegría, A., Craig, M., Langsdorf, S., Löschke, S., Möller, V., Okem, A., Rama, B. (Eds.)]. Cambridge University Press, in press.

Jacobsen, S.B., Wasserburg, G.J. (1980) Sm-Nd Isotopic Evolution of Chondrites. *Earth and Planetary Science Letters* 50, 139–155. https://doi.org/10.1016/0012-821X(80)90125-9

Krumpen, T., Belter, H.J., Boetius, A., Damm, E., Haas, C., Hendricks, S., Nicolaus, M., Nöthig, E.-M., Paul, S., Peeken, I., Ricker, R., Stein, R. (2019) Arctic warming interrupts the Transpolar Drift and affects long-range transport of sea ice and ice-rafted matter. *Scientific Reports* 9, 1–9. https://doi.org/10.1038/s41598-019-41456-y

Krumpen, T., von Albedyll, L., Goessling, H.F., Hendricks, S., Juhls, B., Spreen, G., Willmes, S., Belter, H.J., Dethloff, K., Haas, C., Kaleschke, L., Katlein, C., Tian-Kunze, X., Ricker, R., Rostosky, P., Rückert, J., Singha, S., Sokolova, J. (2021) MOSAiC drift expedition from October 2019 to July 2020: sea ice conditions from space and comparison with previous years. *The Cryosphere* 15, 3897–3920. https://doi.org/10.5194/tc-15-3897-2021

Laukert, G., Frank, M., Bauch, D., Hathorne, E.C., Rabe, B., von Appen, W.-J., Wegner, C., Zieringer, M., Kassens, H. (2017a) Ocean circulation and freshwater pathways in the Arctic Mediterranean based on a combined Nd isotope, REE and oxygen isotope section across Fram Strait. *Geochimica et Cosmochimica Acta* 202, 285–309. https://doi.org/10.1016/j.gca.2016.12.028

Laukert, G., Frank, M., Bauch, D., Hathorne, E.C., Gutjahr, M., Janout, M., Hölemann, J. (2017b) Transport and transformation of riverine neodymium isotope and rare earth element signatures in high latitude estuaries: a case study from the Laptev Sea. *Earth and Planetary Science Letters* 477, 205–217. https://doi.org/10.1016/j.epsl.2017.08.010

Laukert, G., Frank, M., Hathorne, E.C., Krumpen, T., Rabe, B., Bauch, D., Werner, K., Peeken, I., Kassens, K. (2017c) Pathways of Siberian freshwater and sea ice in the Arctic Ocean traced with radiogenic neodymium isotopes and rare earth elements. *Polarforschung* 87, 3–13. https://doi.org/10.2312/polarforschung.87.1.3

Laukert, G., Dreyer, J., Frank, M., Hathorne, E.C., Meulenbroek, K. (2018) Greenland-sourced freshwater traced by radiogenic neodymium isotopes and rare earth elements on the North-East Greenland Shelf. *Goldschmidt Abstracts* 2018, 1419. https://goldschmidtabstracts.info/2018/1419.pdf

Laukert, G., Makhotin, M., Petrova, M.V., Frank, M., Hathorne, E.C., Bauch, D., Böning, P., Kassens, H. (2019) Water mass transformation in the Barents Sea inferred from radiogenic neodymium isotopes, rare earth elements and stable oxygen isotopes. *Chemical Geology* 511, 416–430. https://doi.org/10.1016/j.chemgeo.2018.10.002

Paffrath, R., Laukert, G., Bauch, D., Rutgers van der Loeff, M., Pahnke, K. (2021) Separating individual contributions of major Siberian rivers in the Transpolar Drift of the Arctic Ocean. *Scientific Reports* 11, 8216. https://doi.org/10.1038/s41598-021-86948-y

Porcelli, D., Andersson, P.S., Baskaran, M., Frank, M., Bjork, G., Semiletov, I. (2009) The distribution of neodymium isotopes in Arctic Ocean basins. *Geochimica et Cosmochimica Acta* 73, 2645–2659. https://doi.org/10.1016/j.gca.2008.11.046

Neodymium isotopes trace marine provenance of Arctic sea ice

G. Laukert, I. Peeken, D. Bauch, T. Krumpen, E.C. Hathorne, K. Werner, M. Gutjahr, M. Frank

Supplementary Information

The Supplementary Information includes:

- Neodymium Isotope Systematics in the Arctic Ocean
- Sample Collection and Preparation
- Laboratory Analyses
- Back-tracking of Sea Ice Based on Satellite Data
- Tables S-1 to S-8
- Figures S-1 to S-5
- Supplementary Information References

Neodymium Isotope Systematics in the Arctic Ocean

The isotopic composition of neodymium (Nd) is commonly expressed as $\varepsilon_{Nd} = \{(^{143}Nd/^{144}Nd)_{sample}/(^{143}Nd/^{144}Nd)_{CHUR} - 1\} \times 10^4$, with CHUR = 0.512638 (Jacobsen and Wasserburg 1980). In rocks, ε_{Nd} ranges from −56 to +11 on the global scale (Lacan *et al.*, 2012; van de Flierdt *et al.*, 2016). This variability is caused by the fractionation between Nd and samarium (Sm) during magmatic processes and the decay of ^{147}Sm to ^{143}Nd, which together result in more radiogenic (*i.e.* more positive) ε_{Nd} signatures in young mantle-derived rocks compared to old continental rocks. Water masses acquire these distinct rock signatures mainly at the land-ocean interface after their introduction through weathered continental material via rivers, groundwater and coastal erosion. Tracing of the seawater (*i.e.* dissolved) signatures and the water masses they are carried by is enabled by the quasi-conservative behaviour of Nd in the open ocean (Frank, 2002; Goldstein and Hemming, 2003) and its intermediate average oceanic residence time of several hundred years (Tachikawa *et al.*, 2003; Arsouze *et al.*, 2009; Rempfer *et al.*, 2011; Pöppelmeier *et al.*, 2020).

In the Arctic Ocean, seawater ε_{Nd} signatures have been attributed primarily to terrestrial inputs and water mass circulation and mixing, whereas ε_{Nd} changes associated with seawater-particle interactions have been shown to be restricted to certain shelf regions (Andersson *et al.*, 2008; Porcelli *et al.*, 2009; Charette *et al.*, 2016; Laukert *et al.*, 2017a, 2017b, 2017c, 2019; Paffrath *et al.*, 2021a, 2021b). The main Nd sources of the Arctic Ocean and their ε_{Nd} are shown in Fig. S-1. The Atlantic-derived waters dominate the Nd budget with ε_{Nd} signatures around −13 at the Iceland-Scotland Ridge and the Denmark Strait (Laukert *et al.*, 2017a and references therein). Pacific-derived waters entering the Arctic Ocean through the Bering Strait have more radiogenic ε_{Nd} signatures around −3 to −2, which are slightly modified in the Chukchi Sea resulting in ε_{Nd} signatures of −5.5 entering the open Arctic Ocean (Charette *et al.*, 2016).

Freshwater introduced by the various Arctic rivers has a wide range in ε_{Nd} compositions from −17 to −5 (Porcelli *et al.*, 2009; Zimmermann *et al.*, 2009; Persson *et al.*, 2011; Laukert *et al.*, 2017a, 2017b). Significantly less radiogenic signatures (<−17) are only introduced through discharge from Greenland and the Canadian Arctic Archipelago (Filippova *et al.*, 2017; Laukert *et al.*, 2018; Grenier *et al.*, 2022). The sea ice cover prevents aeolian Nd to reach the entire Arctic Ocean in winter and year-round in the central Arctic Ocean. Instead, atmospheric Nd is likely trapped in snow deposited on sea ice and released only during the melt season.

All published ε_{Nd} data for surface seawater are shown in Figure S-1 in addition to major external Nd sources. Despite considerable mixing, laterally and vertically separated contributions from the Lena and Yenisei/Ob rivers were recently identified in the central Arctic Ocean and considered as different source clusters of the Transpolar Drift (Paffrath *et al.*, 2021a). Similar provenance tracer characteristics have been observed in the northern Laptev Sea (Laukert *et al.*, 2017b), suggesting that the Laptev Sea is the main source region for freshwater, nutrients, and trace elements transported via the Transpolar Drift. Depending on the wind fields, the Lena plume is transported either northward or eastward (Janout *et al.*, 2020), resulting in spatiotemporal variability in the distribution of source tracers within the Transpolar Drift.

Sample Collection and Preparation

Sampling of sea ice, snow and seawater was carried out during the PS85 cruise with the RV *Polarstern* in the Fram Strait in June and July 2014. At each ice station, a designated coring site was assigned and, if present, the snow was sampled prior to the drilling of the sea ice cores. Several ice cores free of ice rafted detrital material based on visual inspection were taken at each station, one of which was used for high-resolution temperature and salinity profiles and another one for tracer analysis. Nitrile gloves were used during sampling and cores were drilled with a Kovacs 9 cm diameter corer (Kovacs Enterprise, Roseburg, USA). The temperature of the ice was directly measured on the floe by drilling into the ice and determining the temperature every 5 cm with a Testo 720 RTD thermometer. Thereafter the core was sectioned in 10 cm pieces and weighted to calculate the brine volume. After melting the salinity was determined with a WTW salinity probe. The ice cores were immediately transferred into plastic bags (LDPE tube films by Rische and Herfurth) and stored at −20 °C. Snow was collected with an acid-cleaned plastic shovel and stored at −20 °C in acid-cleaned plastic bags. A SBE32 rosette water sampler equipped with 24 Niskin-type sample bottles (12 L) was used for collection of the seawater samples, which were directly filtered through AcroPakTM500 Capsules with Supor Membrane (pore size, 0.8/0.2µm) filter cartridges, collected in 20 L acid-cleaned LDPE-containers and stored on board.

The frozen sea ice samples were transported to GEOMAR and processed in the clean room laboratory (MK-Versuchsanlagen, class 100 hoods) immediately after removal from the freezer. All mechanical work on the ice cores was carried out on a clean plastic table covered with acid-cleaned Teflon foil. To remove contaminants from the surfaces of the sea ice samples, the ice cores were rinsed with deionised water (18.2 MΩ cm, Milli-Q system) at a temperature of ~20 °C for about 15 seconds. Subsequently, the top surface of the ice cores was scraped off with a custom-made titanium grade 1 chisel. The cores were then split into several pieces with a titanium grade 1 hammer and put into acid-cleaned LDPE-buckets with closed plastic lids for melting. No release of brine water was observed throughout the sample processing period. The ice melted within ~12 h or less, and the meltwater samples were filtered through Merck Millipore® 0.45 µm cellulose acetate filters immediately after the last piece of ice melted. The meltwater was then transferred to acid-cleaned LDPE cubitainers. The snow samples were treated similarly to the sea-ice samples, except that they were not rinsed with deionised water (this was not necessary given that the plastic bags in which the snow was stored were acid-cleaned). After sub-sampling of sea ice and snow meltwater for salinity and stable oxygen isotope analysis as well as REE ultrafiltration, the filtered sea ice, snow and seawater samples were acidified to pH ≈ 2.2 with ultra-pure concentrated hydrochloric acid and at least 48 h for equilibration were given before another aliquot was separated into an acid-cleaned LDPE-bottle for REE concentration and other analyses.

Ultrafiltration of the sea ice and snow meltwater for REE analysis was performed immediately after initial filtration through Merck Millipore 0.45 µm cellulose acetate filters. Amicon® Ultra-15 centrifugal filter units with a volume of 15 mL and either 3000 or 30,000 Nominal Molecular Weight Limit (*i.e.* 3 or 30 kDa) were used. The tubes were first acid-cleaned and deionised water (18.2 MΩ cm, Milli-Q system) was filtered twice before the actual sample was filtered and collected. Filtration was carried out at 3500 rpm for 20 minutes. The samples were then acidified to a pH of ~2.2 with ultra-pure concentrated hydrochloric acid before further processing.

Laboratory Analyses

Radiogenic neodymium isotopes

The entire pre-concentration, purification and measurement techniques reported here strictly followed approved GEOTRACES protocols and were confirmed through participation in the international GEOTRACES inter-calibration study (van de Flierdt *et al.*, 2012). To each seawater, sea ice and snow sample trace metal clean $FeCl_3$ solution was added (~200 mg Fe/mL) and the samples were left for equilibration for 24 h before trace metal clean ammonia solution (25 %, Merck Suprapur®) was added to raise the pH to 7.5–8.0. After 48 h, the co-precipitated trace elements settled to the bottom of the cubitainers together with FeOOH and the supernatant water was syphoned off. The precipitates were centrifuged and rinsed three times with deionised water (MilliQ, 18.2 MΩcm) in 50 mL centrifuge tubes to remove major ions, transferred into 60 mL PFA vials with 6 M HCl and then evaporated to dryness. To remove organic components, the samples were treated with aqua regia at 120 °C for 24 h. After evaporation to dryness, the samples were dissolved in 6 M HCl and the sample in solution was washed with pre-cleaned di-ethyl ether to remove 99 % of the Fe (Stichel *et al.*, 2012), dried down and dissolved in 1 M HCl for column chemistry. The REEs were separated from matrix elements through cation exchange chromatography (BIORAD®, AG50W-X8 resin, 200–400 µm mesh-size, 1.4 mL resin bed) with a slightly modified separation scheme of Stichel *et al.* (2012), where instead of a mixture of HCl and HF acids only HCl was used as a reagent. Nd was further purified from the other REEs for isotope measurements using Eichrom® LN-Spec resin (2 mL, 50–100 µm) following previously established procedures (Pin and Zalduegui, 1997; Le Fèvre and Pin, 2005). To destroy residual traces of the resin and organic compounds the samples were finally treated with concentrated quartz-distilled HNO_3 before Nd isotope measurements.

The $^{143}Nd/^{144}Nd$ ratios were measured on a Neptune Plus MC-ICP-MS (40 cycles at 4 s, 10^{12} Ω resistors assigned to masses 143 and 146) and were double-corrected for instrumental mass bias to $^{146}Nd/^{144}Nd = 0.7219$ and to $^{142}Nd/^{144}Nd = 1.141876$, provided that the ^{142}Ce beam intensity was sufficiently low (Vance and Thirwall, 2002), monitored via ensuring a raw measured $^{140}Ce/^{144}Nd < 1$ (*i.e.* $Ce/Nd < 0.3$) for each sample and standard solution. Isobaric interferences between ^{144}Sm and ^{144}Nd were corrected by measuring the abundance of the interference free isotope ^{147}Sm and by calculating the potential ^{144}Sm contribution on mass 144 from the natural abundance of Sm. The $^{143}Nd/^{144}Nd$ ratios of all samples were normalised to the accepted JNdi-1 standard value of 0.512115 (Tanaka *et al.*, 2000). The external reproducibility of the Nd isotope measurements as estimated by repeated measurements of the JNdi-1 standard at concentrations matched to fit to those of the samples (between 0.2 and 3 ng, $n = 4$) ranged between 0.5 and 3.6 ε_{Nd} units (2 s.d.). Some of the snow and sea ice samples had a low Nd yield likely due to loss during column chemistry. The procedural laboratory blanks ($n = 3$) had <10 pg, which corresponds to <6 % of the lowest Nd concentration used for the isotope measurements. Blank corrections were not applied, and blank contributions are provided in % in Tables S-2 and S-3.

Rare earth element concentrations

The REE concentrations were determined for filtered and ultrafiltered samples using an online pre-concentration (OP) ICP-MS technique at GEOMAR by directly coupling a "seaFAST" system (Elemental Scientific Inc., Nebraska, USA) to an ICP-MS (Agilent 7500ce) (Hathorne *et al.*, 2012). The method of Hathorne *et al.* (2012) was further improved by using an 8 mL sample loop and by preparation of calibration standards with a mixed REE solution of a seawater-like composition in a natural seawater matrix (Osborne *et al.*, 2015). Repeated measurements of GEOTRACES intercalibration sample BATS 2000m (van de Flierdt *et al.*, 2012) and the diluted (500×) reference material SLRS-4 were used to monitor the external reproducibility, which based on BATS 2000m was better than ~6 %, ~7 % and ~11 % for the LREEs, MREEs and HREEs, respectively, and based on SLRS-4 was better than ~8 %, ~18 % and ~34 %, respectively. We diluted SLRS-4 to monitor the accuracy and precision of measurements of snow and sea ice samples with similarly low REE concentrations. The measured REE of SLRS-4 and BATS 2000m agree well with literature values (Table S-8). The procedural laboratory blanks (n = 3, filtered and ultrafiltered) had similar REE concentrations on average corresponding to less than 5 % of sea ice and snow samples analysed, except for Ce which was on average ~7 % (Table S-8).

Stable oxygen isotopes and sample salinity

Oxygen isotope compositions were analysed at the Stable Isotope Laboratory of the College of Earth, Ocean, and Atmospheric Sciences at Oregon State University (Corvallis, USA) applying a CO_2-water isotope equilibration technique (Epstein and Mayeda, 1953) on at least two subsamples on a DeltaPlusXL instrument. The external reproducibility for the $\delta^{18}O$ measurements was ±0.04 ‰ or better and the measured $^{18}O/^{16}O$ ratio is provided as a deviation from Vienna Standard Mean Ocean Water in the δ-notation (Craig, 1961). Sample salinity was determined with an AutoSal 8400A salinometer at GEOMAR with a precision of ±0.003 and an accuracy better than ±0.005.

Back-tracking of Sea Ice Based on Satellite Data

Pathways, age and source area of sampled sea ice were investigated with the AWI IceTrack system (Krumpen *et al.*, 2020). The low-resolution sea ice drift product OSI-405-c from the Ocean and Sea Ice Satellite Application Facility (OSI SAF; Lavergne, 2016; 62.5 × 62.5 km grid spacing) is used to trace sea ice backward in time until sea-ice concentration at a specific location drops below a predefined threshold (here 50 %) and we assume the ice to be formed. The sea-ice concentration product is based on the 85 GHz Special Sensor Microwave/Imager (SSM/I) and provided by CERSAT (Ezraty *et al.*, 2007; 12.5 km resolution). To assess the accuracy of this Lagrangian tracking approach, Krumpen *et al.* (2019) reconstructed the pathways of 56 GPS buoys deployed between 2011 and 2016 in the central Arctic Ocean. The displacement between real and virtual tracks is rather small (36 ± 20 km after 200 days). However, the accuracy of the method is lower in Fram Strait, likely due to a general underestimation of drift velocities by low-resolution satellite products in this area (Krumpen *et al.*, 2021) (Fig. 2c). Therefore, in this study, the sampled sea ice in Fram Strait was first manually tracked for a short distance using optical satellite data (MODIS - provided via https://worldview.earthdata.nasa.gov) before tracking was continued with IceTrack.

Supplementary Tables

Table S-1 Sea ice and snow sampling and accompanying information.

Table S-2 Salinity, $\delta^{18}O$ and dissolved (<0.45 μm) ε_{Nd} compositions of sea ice.

Table S-3 Salinity, $\delta^{18}O$ and dissolved (<0.45 μm) ε_{Nd} compositions of snow.

Table S-4 Dissolved (<0.45 μm) and truly dissolved (<30 kDa and 3 kDa) REE concentrations of sea ice.

Table S-5 Dissolved (<0.45 μm) and truly dissolved (<30 kDa and 3 kDa) REE concentrations of snow.

Table S-6 Dissolved (<0.2 μm) ε_{Nd} compositions and REE concentrations of surface seawater.

Table S-7 High-resolution temperature and salinity profiles of sea ice cores from same stations.

Table S-8 REE concentrations of reference materials SLRS-4 (500× dilution), BATS 2000m and blanks.

Tables S-1 to S-8 are available for download (Excel) from the online version of the article at https://doi.org/10.7185/geochemlet.2220.

Supplementary Figures

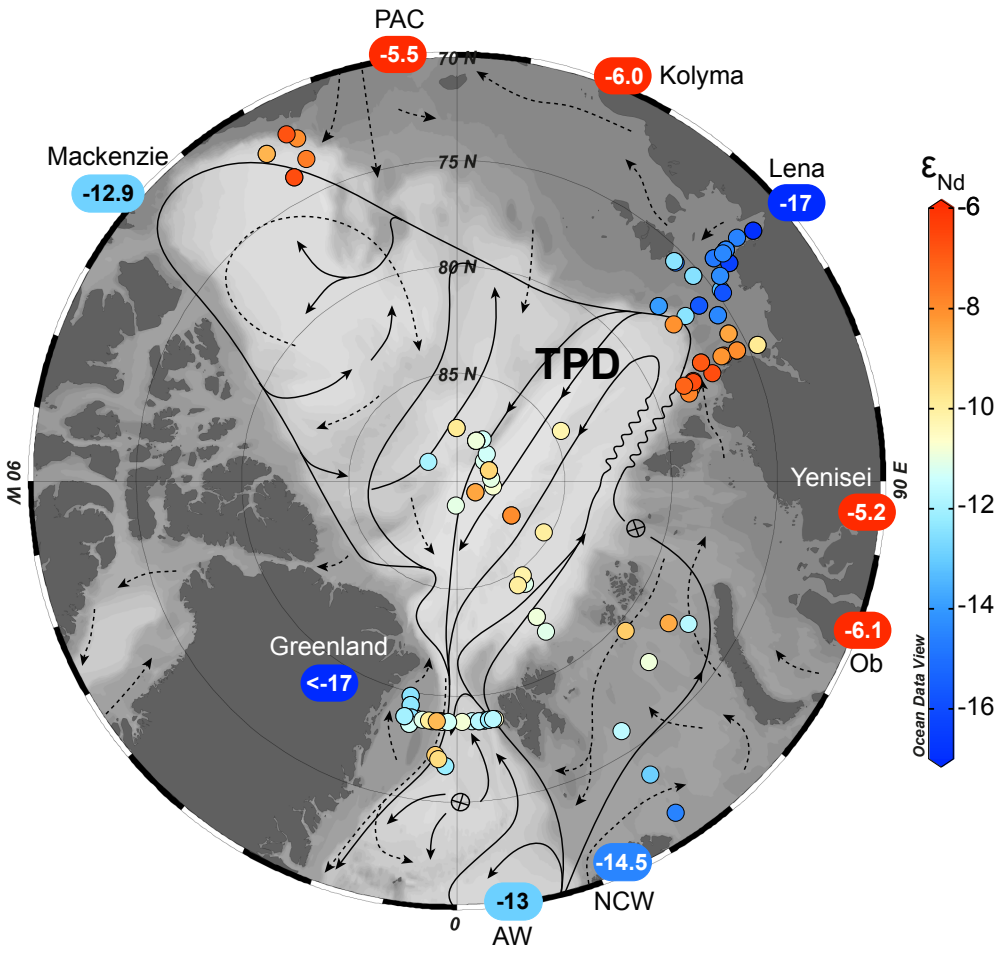

Figure S-1 Bathymetric map of the Arctic Ocean (IBCAO; Jakobsson *et al.*, 2012) with major Nd sources and their ε_{Nd} signatures as well as published surface seawater ε_{Nd} data (Andersson *et al.*, 2008; Porcelli *et al.*, 2009; Zimmermann *et al.*, 2009; Persson *et al.*, 2011; Charette *et al.*, 2016; Laukert *et al.*, 2017a, 2017b; Paffrath *et al.*, 2021a). The Transpolar Drift (TPD) and the general circulation pattern of surface (dashed black arrows) and AW (black arrows) waters are shown in addition (modified after Rudels *et al.*, 2012). The known Nd sources are Atlantic-derived waters (AW) entering through the Iceland-Scotland Ridge and the Denmark Strait, Norwegian Coastal Water (NCW), modified Pacific-derived waters (PAC), major Siberian Rivers (Ob, Yenisei, Lena, Kolyma), and the Mackenzie River.

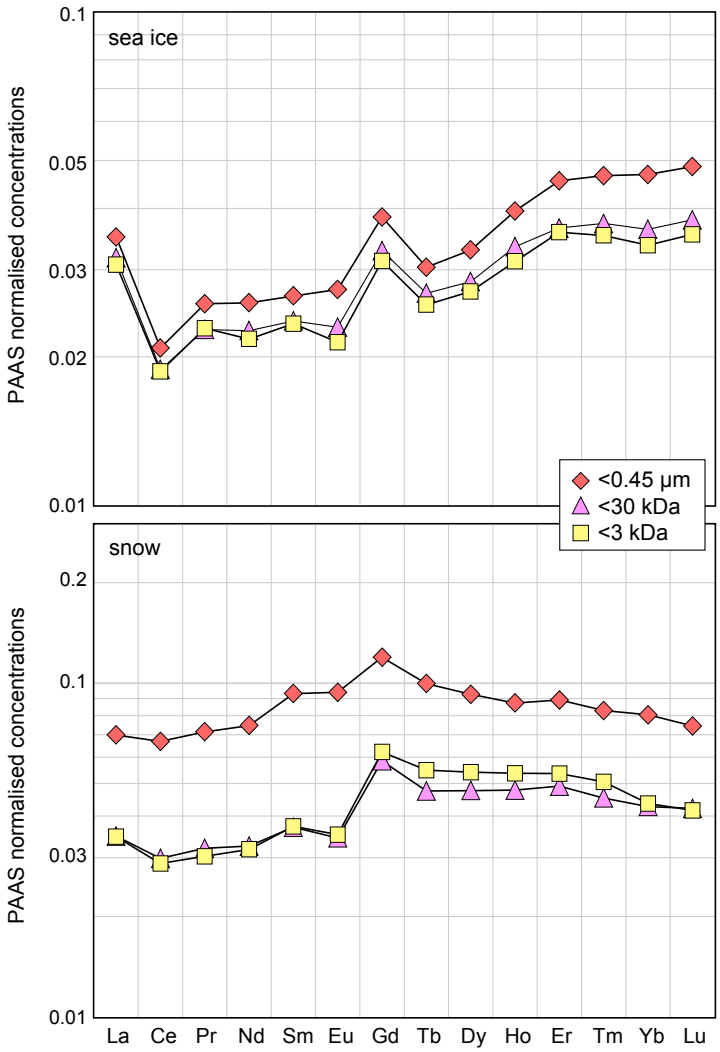

Figure S-2 Averaged rare earth element (REE) concentrations of the different size pools in sea ice (upper figure) and snow (lower figure) samples normalised to Post Archaean Australian Shale ($\times 10^6$; McLennan, 2001).

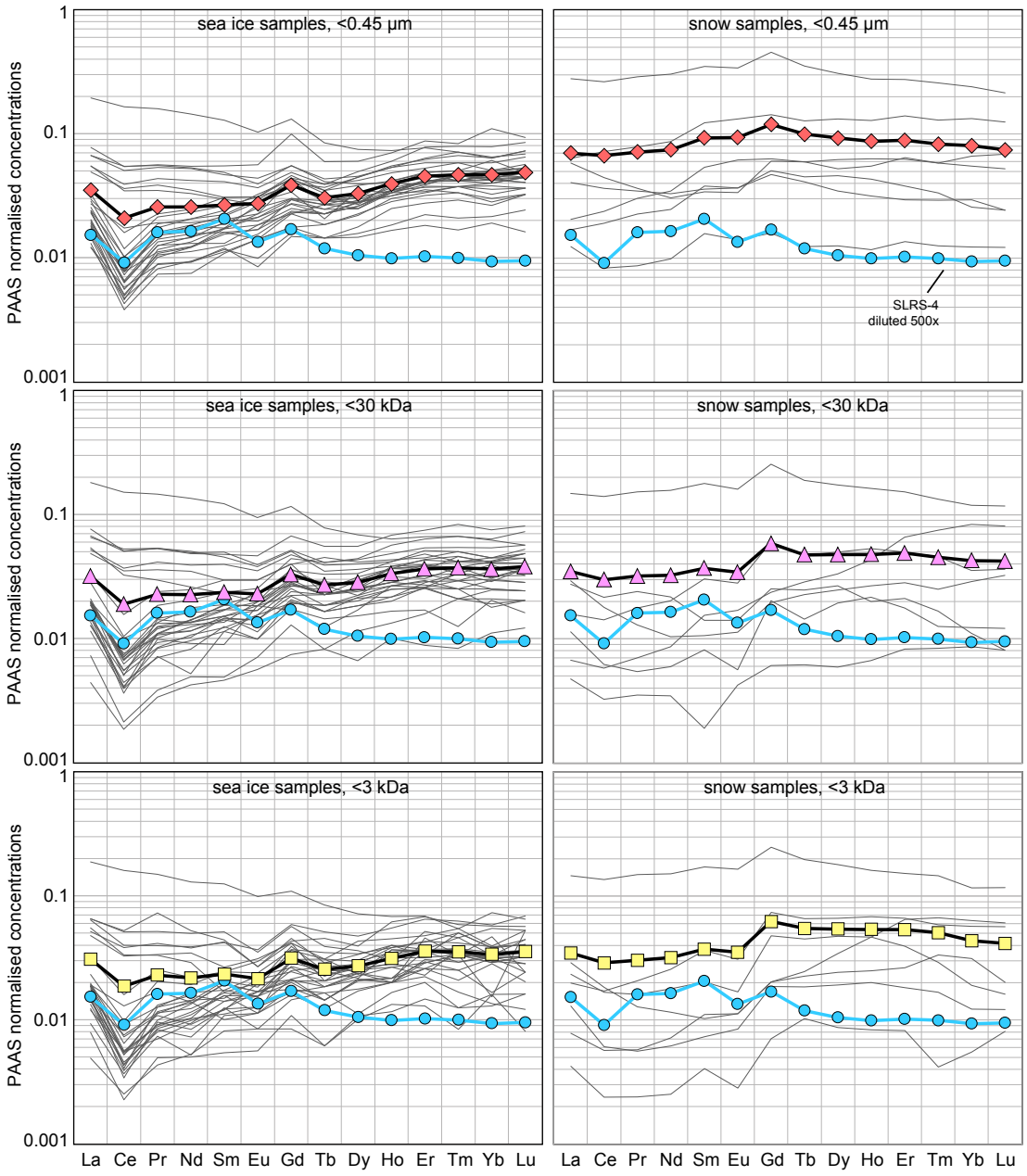

Figure S-3 Rare earth element (REE) concentrations of all sea ice and snow samples normalised to Post Archaean Australian Shale ($\times 10^6$; McLennan, 2001) with the corresponding averages (same colours as in Fig. S-1). For comparison, the reference material SLRS-4 is shown (500× dilution).

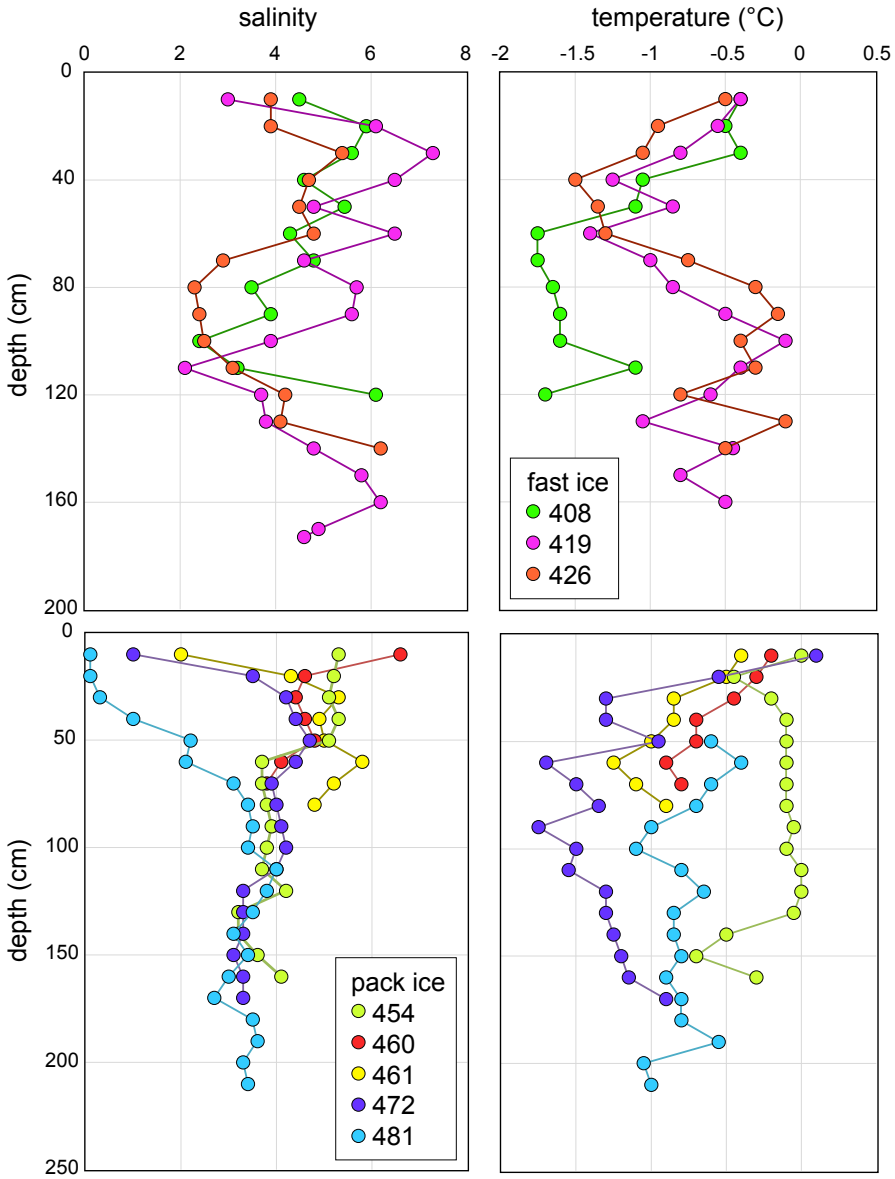

Figure S-4 High-resolution temperature and salinity profiles of fast ice (upper figures) and pack ice (lower figures). Temperature was averaged from 5 cm intervals.

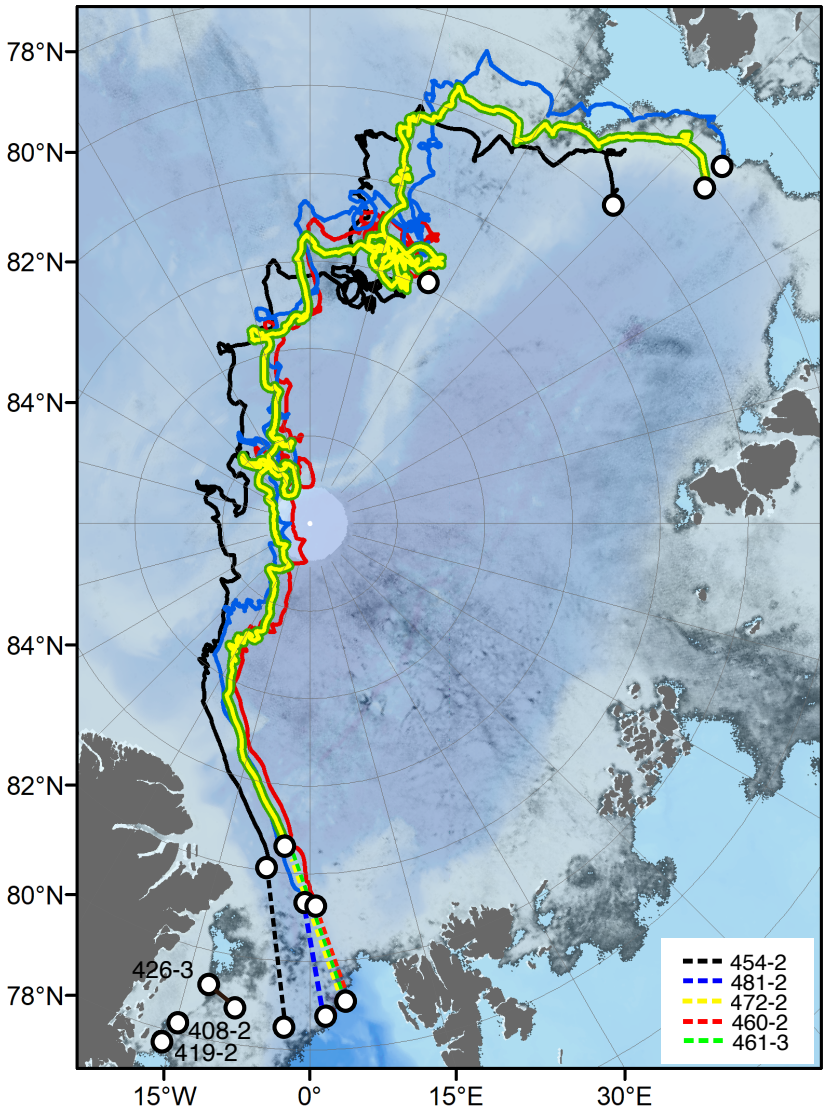

Figure S-5 Reconstructed sea ice origin and drift trajectories from short-distance manual tracking (all fast ice stations and dashed lines for pack ice) using optical satellite data (MODIS - provided via https://worldview.earthdata.nasa.gov) and long-distance tracking (solid lines, only pack ice) based on the AWI IceTrack system (Krumpen *et al.*, 2020).

Supplementary Information References

Andersson, P.S., Porcelli, D., Frank, M., Bjork, G., Dahlqvist, R., Gustafsson, O. (2008) Neodymium isotopes in seawater from the Barents Sea and Fram Strait Arctic-Atlantic gateways. *Geochimica et Cosmochimica Acta* 72, 2854–2867. https://doi.org/10.1016/j.gca.2008.04.008

Arsouze, T., Dutay, J.-C., Lacan, F., Jeandel, C. (2009) Reconstructing the Nd oceanic cycle using a coupled dynamical – biogeochemical model. *Biogeosciences* 6, 2829–2846. https://doi.org/10.5194/bg-6-2829-2009

Charette, M.A., Lam, P.J., Lohan, M.C., Kwon, E.Y., Hatje, V., *et al*. (2016) Coastal ocean and shelf-sea biogeochemical cycling of trace elements and isotopes: lessons learned from GEOTRACES. *Philosophical Transactions of the Royal Society A: Mathematical, Physical and Engineering Sciences* 374, 20160076. https://doi.org/10.1098/rsta.2016.0076

Craig, H. (1961) Isotopic Variations in Meteoric Waters. *Science* 133, 1702–1703. https://doi.org/10.1126/science.133.3465.1702

Epstein, S., Mayeda, T. (1953) Variation of O^{18} content of waters from natural sources. *Geochimica et Cosmochimica Acta* 4, 213–224. https://doi.org/10.1016/0016-7037(53)90051-9

Ezraty, R., Girard-Ardhuin, F., Piolle, J.F., Kaleschke, L., Heygster, G. (2007) *Arctic and Antarctic Sea Ice Concentration and Arctic Sea Ice Drift Estimated from Special Sensor Microwave Data – User's manual V2.1*. Technical Report, Département d'Océanographie Physique et Spatiale, IFREMER, Brest, France.

Filippova, A., Frank, M., Kienast, M., Rickli, J., Hathorne, E.C., Yashayaev, I.M., Pahnke, K. (2017) Water mass circulation and weathering inputs in the Labrador Sea based on coupled Hf–Nd isotope compositions and rare earth element distributions. *Geochimica et Cosmochimica Acta* 199, 164–184. https://doi.org/10.1016/j.gca.2016.11.024

Frank, M. (2002) Radiogenic isotopes: tracers of past ocean circulation and erosional input. *Reviews of Geophysics* 40, 1–38. https://doi.org/10.1029/2000RG000094

Goldstein, S.L., Hemming, S.R. (2003) 6.17 - Long-lived Isotopic Tracers in Oceanography, Paleoceanography, and Ice-sheet Dynamics. In: Holland, H.D., Turekian, K.K. (Eds.) *Treatise on Geochemistry, Volume 6: The Oceans and Marine Geochemistry*. First Edition, Elsevier, Amsterdam, 453–489. https://doi.org/10.1016/B0-08-043751-6/06179-X

Grenier, M., Brown, K.A., Colombo, M., Belhadj, M., Baconnais, I., Pham, V., Soon, M., Myers, P.G., Jeandel, C., François, R. (2022) Controlling factors and impacts of river-borne neodymium isotope signatures and rare earth element concentrations supplied to the Canadian Arctic Archipelago. *Earth and Planetary Science Letters* 578, 117341. https://doi.org/10.1016/j.epsl.2021.117341

Hathorne, E.C., Haley, B.A., Stichel, T., Grasse, P., Zieringer, M., Frank, M. (2012) Online preconcentration ICP-MS analysis of rare earth elements in seawater. *Geochemistry, Geophysics, Geosystems* 13, Q01020. https://doi.org/10.1029/2011GC003907

Jacobsen, S.B., Wasserburg, G.J. (1980) Sm-Nd Isotopic Evolution of Chondrites. *Earth and Planetary Science Letters* 50, 139–155. https://doi.org/10.1016/0012-821X(80)90125-9

Jakobsson, M., Mayer, L., Coakley, B., Dowdeswell, J.A., Forbes, S., *et al*. (2012) The International Bathymetric Chart of the Arctic Ocean (IBCAO) Version 3.0. *Geophysical Research Letters* 39, L12609. https://doi.org/10.1029/2012GL052219

Janout, M.A., Hölemann, J., Laukert, G., Smirnov, A., Krumpen, T., Bauch, D., Timokhov, L. (2020) On the Variability of Stratification in the Freshwater-Influenced Laptev Sea Region. *Frontiers in Marine Science* 7, 543489. https://doi.org/10.3389/fmars.2020.543489

Krumpen, T., Belter, H.J., Boetius, A., Damm, E., Haas, C., Hendricks, S., Nicolaus, M., Nöthig, E.-M., Paul, S., Peeken, I., Ricker, R., Stein, R. (2019) Arctic warming interrupts the Transpolar Drift and affects long-range transport of sea ice and ice-rafted matter. *Scientific Reports* 9, 1–9. https://doi.org/10.1038/s41598-019-41456-y

Krumpen, T., Birrien, F., Kauker, F., Rackow, T., von Albedyll, L., *et al*. (2020) The MOSAiC ice floe: sediment-laden survivor from the Siberian shelf. *The Cryosphere* 14, 2173–2187. https://doi.org/10.5194/tc-14-2173-2020

Krumpen, T., von Albedyll, L., Goessling, H.F., Hendricks, S., Juhls, B., Spreen, G., Willmes, S., Belter, H.J., Dethloff, K., Haas, C., Kaleschke, L., Katlein, C., Tian-Kunze, X., Ricker, R., Rostosky, P., Rückert, J., Singha, S., Sokolova, J. (2021) MOSAiC drift expedition from October 2019 to July 2020: sea ice conditions from space and comparison with previous years. *The Cryosphere* 15, 3897–3920. https://doi.org/10.5194/tc-15-3897-2021

Lacan, F., Tachikawa, K., Jeandel, C. (2012) Neodymium isotopic composition of the oceans: A compilation of seawater data. *Chemical Geology* 300–301, 177–184. https://doi.org/10.1016/j.chemgeo.2012.01.019

Lavergne, T. (2016) *Validation and Monitoring of the OSI SAF Low Resolution Sea Ice Drift Product (v5)*. The EUMETSAT Network of Satellite Application Facilities, Technical Report SAF/OSI/CDOP/Met.no/T&V/RP/131. https://doi.org/10.13140/RG.2.1.4155.5449

Laukert, G., Frank, M., Bauch, D., Hathorne, E.C., Rabe, B., von Appen, W.-J., Wegner, C., Zieringer, M., Kassens, H. (2017a) Ocean circulation and freshwater pathways in the Arctic Mediterranean based on a combined Nd isotope, REE and oxygen isotope section across Fram Strait. *Geochimica et Cosmochimica Acta* 202, 285–309. https://doi.org/10.1016/j.gca.2016.12.028

Laukert, G., Frank, M., Bauch, D., Hathorne, E.C., Gutjahr, M., Janout, M., Hölemann, J. (2017b) Transport and transformation of riverine neodymium isotope and rare earth element signatures in high latitude estuaries: a case study from the Laptev Sea. *Earth and Planetary Science Letters* 477, 205–217. https://doi.org/10.1016/j.epsl.2017.08.010

Laukert, G., Frank, M., Hathorne, E.C., Krumpen, T., Rabe, B., Bauch, D., Werner, K., Peeken, I., Kassens, K. (2017c) Pathways of Siberian freshwater and sea ice in the Arctic Ocean traced with radiogenic neodymium isotopes and rare earth elements. *Polarforschung* 87, 3–13. https://doi.org/10.2312/polarforschung.87.1.3

Laukert, G., Dreyer, J., Frank, M., Hathorne, E.C., Meulenbroek, K. (2018) Greenland-sourced freshwater traced by radiogenic neodymium isotopes and rare earth elements on the North-East Greenland Shelf. *Goldschmidt Abstracts* 2018, 1419. https://goldschmidtabstracts.info/2018/1419.pdf

Laukert, G., Makhotin, M., Petrova, M.V., Frank, M., Hathorne, E.C., Bauch, D., Böning, P., Kassens, H. (2019) Water mass transformation in the Barents Sea inferred from radiogenic neodymium isotopes, rare earth elements and stable oxygen isotopes. *Chemical Geology* 511, 416–430. https://doi.org/10.1016/j.chemgeo.2018.10.002

Le Fèvre, B., Pin, C. (2005) A straightforward separation scheme for concomitant Lu–Hf and Sm–Nd isotope ratio and isotope dilution analysis. *Analytica Chimica Acta* 543, 209–221. https://doi.org/10.1016/j.aca.2005.04.044

McLennan, S.M. (2001) Relationships between the trace element composition of sedimentary rocks and upper continental crust. *Geochemistry, Geophysics, Geosystems* 2, 2000GC000109. https://doi.org/10.1029/2000GC000109

Osborne, A.H., Haley, B.A., Hathorne, E.C., Plancherel, Y., Frank, M. (2015) Rare earth element distribution in Caribbean seawater: Continental inputs versus lateral transport of distinct REE compositions in subsurface water masses. *Marine Chemistry* 177, 172–183. https://doi.org/10.1016/j.marchem.2015.03.013

Paffrath, R., Laukert, G., Bauch, D., Rutgers van der Loeff, M., Pahnke, K. (2021a) Separating individual contributions of major Siberian rivers in the Transpolar Drift of the Arctic Ocean. *Scientific Reports* 11, 8216. https://doi.org/10.1038/s41598-021-86948-y

Paffrath, R., Pahnke, K., Böning, P., Rutgers van der Loeff, M., Valk, O., Gdaniec, S., Planquette, H. (2021b) Seawater-particle interactions of rare earth elements and neodymium isotopes in the deep central Arctic Ocean. *Journal of Geophysical Research: Oceans* 126, e2021JC017423. https://doi.org/10.1029/2021JC017423

Persson, P.O., Andersson, P.S., Porcelli, D., Semiletov, I. (2011) The influence of Lena River water inflow and shelf sediment-sea water exchange for the Nd isotopic composition in the Laptev Sea and Arctic Ocean. *EGU General Assembly Conference Abstracts* 13, EGU2011-672.

Pin, C., Zalduegui, J.F.S. (1997) Sequential separation of light rare-earth elements, thorium and uranium by miniaturized extraction chromatography: Application to isotopic analyses of silicate rocks. *Analytica Chimica Acta* 339, 79–89. https://doi.org/10.1016/S0003-2670(96)00499-0

Porcelli, D., Andersson, P.S., Baskaran, M., Frank, M., Bjork, G., Semiletov, I. (2009) The distribution of neodymium isotopes in Arctic Ocean basins. *Geochimica et Cosmochimica Acta* 73, 2645–2659. https://doi.org/10.1016/j.gca.2008.11.046

Pöppelmeier, F., Scheen, J., Blaser, P., Lippold, J., Gutjahr, M., Stocker, T.F. (2020) Influence of Elevated Nd Fluxes on the Northern Nd Isotope End Member of the Atlantic During the Early Holocene. *Paleoceanography and Paleoclimatology*, 35, e2020PA003973. https://doi.org/10.1029/2020PA003973

Rempfer, J., Stocker, T.F., Joos, F., Dutay, J.C., Siddall, M. (2011) Modelling Nd-isotopes with a coarse resolution ocean circulation model: Sensitivities to model parameters and source/sink distributions. *Geochimica et Cosmochimica Acta* 75, 5927–5950. https://doi.org/10.1016/j.gca.2011.07.044

Rudels, B., Anderson, L., Eriksson, P., Fahrbach, E., Jakobsson, M., Jones, E.P., Melling, H., Prinsenberg, S., Schauer, U., Yao, T. (2012) Observations in the Ocean. In: Lemke, P., Jacobi, H.W. (Eds.) *Atmospheric and Oceanographic Sciences Library, Volume 43: Arctic Climate Change*. Springer Dordrecht, 117–198. https://doi.org/10.1007/978-94-007-2027-5_4

Stichel, T., Frank, M., Rickli, J., Haley, B.A. (2012) The hafnium and neodymium isotope composition of seawater in the Atlantic sector of the Southern Ocean. *Earth and Planetary Science Letters* 317–318, 282–294. https://doi.org/10.1016/j.epsl.2011.11.025
Tachikawa, K., Athias, V., Jeandel, C. (2003) Neodymium budget in the modern ocean and paleo-oceanographic implications. *Journal of Geophysical Research: Oceans* 108, 3254. https://doi.org/10.1029/1999JC000285

Tanaka, T., Togashi, S., Kamioka, H., Amakawa, H., Kagami, H., Hamamoto, T., Yuhara, M., Orihashi, Y., Yoneda, S., Shimizu, H., Kunimaru, T., Takahashi, K., Yanagi, T., Nakano, T., Fujimaki, H., Shinjo, R., Asahara, Y., Tanimizu, M., Dragusanu, C. (2000) JNdi-1: a neodymium isotopic reference in consistency with LaJolla neodymium. *Chemical Geology* 168, 279–281. https://doi.org/10.1016/S0009-2541(00)00198-4

van de Flierdt, T., Pahnke, K., Amakawa, H., Andersson, P.S., Basak, C., *et al*. (2012) GEOTRACES intercalibration of neodymium isotopes and rare earth element concentrations in seawater and suspended particles. Part 1: reproducibility of results for the international intercomparison. *Limnology and Oceanography: Methods* 10, 234–251. https://doi.org/10.4319/lom.2012.10.234

van de Flierdt, T., Griffiths, A.M., Lambelet, M., Little, S.H., Stichel, T., Wilson, D.J. (2016) Neodymium in the oceans: a global database, a regional comparison and implications for palaeoceanographic research. *Philosophical Transactions of the Royal Society A: Mathematical, Physical and Engineering Sciences* 374, 20150293. https://doi.org/10.1098/rsta.2015.0293

Vance, D., Thirlwall, M. (2002) An assessment of mass discrimination in MC-ICPMS using Nd isotopes. *Chemical Geology* 185, 227–240. https://doi.org/10.1016/S0009-2541(01)00402-8

Yeghicheyan, D., Carignan, J., Valladon, M., Bouhnik Le Coz, M., Le Cornec, F., *et al*. (2001) A Compilation of Silicon and Thirty One Trace Elements Measured in the Natural River Water Reference Material SLRS-4 (NRC-CNRC). *Geostandards Newsletter* 25, 465–474. https://doi.org/10.1111/j.1751-908X.2001.tb00617.x

Zimmermann, B., Porcelli, D., Frank, M., Andersson, P.S., Baskaran, M., Lee, D.C., Halliday, A.N. (2009) Hafnium isotopes in Arctic Ocean water. *Geochimica et Cosmochimica Acta* 73, 3218–3233. https://doi.org/10.1016/j.gca.2009.02.028